Region Based Target Detection Approach for Synthetic Aperture Radar Images and Its Parallel Implementation

Fatih Nar*[a], Can Demirkesen[a], O. Erman Okman[a], Mujdat Cetin[b]

[a]SDT Space and Defence Technologies, Galyum Blok No.2 ODTU Teknokent Ankara, Turkey;
[b]Faculty of Engineering and Natural Sciences, Sabanci University, Orhanli-Tuzla, Istanbul, Turkey

ABSTRACT

Automatic target detection (ATD) methods for synthetic aperture radar (SAR) imagery are sensitive to image resolution, target size, clutter complexity, and speckle noise level. However, a robust ATD method needs to be less sensitive to the above factors. In this study, a constant false alarm rate (CFAR) based method is proposed which can perform target detection independent of image resolution and target size even in heterogeneous background clutter. The proposed method is computationally efficient since clutter statistics are calculated only for candidate target regions and a single execution of the method is sufficient for different types of targets having different shapes and sizes. Computational efficiency is further increased by parallelizing the algorithm using OpenMP and NVidia CUDA implementations.

Keywords: Automatic Target Detection, CFAR, SAR, GPU implementation.

1. INTRODUCTION

The demand for automatic interpretation of synthetic aperture radar (SAR) images is increasing due to the rapid increase in the quantity and quality of data acquired by airborne and spaceborne systems. Identifying the existence of an object with different characteristics than the background clutter, i.e., automatic target detection (ATD), has been and continues to be one of the critical problems in automatic SAR image interpretation [1]. Since this is one of the first steps of any recognition process, speed and accuracy of the developed technique is crucial in order to satisfy the requirements of many intelligence and surveillance systems.

Given its importance, ATD is studied by many researchers and a variety of approaches have been proposed in the literature. Among these methods, CFAR based approaches are commonly preferred in the literature since they have reasonable computational requirements, constant false alarm rate, adaptive threshold selection capability, and fast detection performance [2]. Hence, CFAR based techniques are extensively studied in the literature [2-7] and applied in many ATD and automatic target recognition (ATR) applications.

CFAR based ATD methods mainly aim to detect objects while satisfying a predefined false alarm rate under unknown clutter level. To this end, for each pixel in the image, a threshold value is calculated using the pixels in the pre-defined region around the corresponding pixel and that pixel is labeled as target or not based on the calculated threshold. However, these methods assume pre-defined regular shapes for the objects and require approximate knowledge of the size of the objects to be detected. Besides, the clutter regions around potential targets are selected similarly, hence these regions also have regular shapes which may cause some degradation in detection accuracy.

In this study, we propose a CFAR-based ATD approach that adaptively determines the target shape and clutter regions by utilizing a region growing method and performs hypothesis testing based on the background model. Through this procedure, it is possible to detect various types of targets having different shapes and sizes. The proposed method also has no constraints on the approach used for estimating the clutter statistics. Fast execution of ATD is very critical since it is generally the first step in SAR ATR. With this perspective, we have developed an adaptive CFAR method which allows fast target detection since a) clutter statistics are calculated only around candidate target regions which constitute a small percentage of the image, b) only a single execution of the method is sufficient for detecting different types of targets having different shapes and sizes, and c) each step of the proposed method is parallelizable so that it is possible to increase the computational efficiency to its utmost limits. Our experimental analysis demonstrates the improved accuracy provided by our approach as well as speed ups obtained through OpenMP CPU and NVidia CUDA GPU parallel implementations.

This paper is organized as follows. In Section 2, the commonly used traditional CFAR approaches as well as more contemporary CFAR approaches are described. In Section 3, the details of the proposed algorithm are provided and adaptation for parallel implementation is discussed. The experimental results and the performance evaluation of the method are presented in Section 4, and finally, Section 5 concludes the paper.

2. CFAR BASED ATD METHODS

For SAR images, detection performance of a method is determined by the reflectivity difference between the object and the clutter and the reflectivity deviation in the clutter region. Originally, CFAR has been proposed to calculate the clutter statistics and obtain a threshold value to satisfy a constant false alarm rate [8]. By this approach, the targets that are not sufficiently bright or not statistically different comparing to its clutter may be eliminated so that false alarm rate could be kept as low as required, which is a crucial aspect of the ATD and therefore ATR systems.

The two parameter CFAR (Cell Averaging CFAR, CA-CFAR) [8] assumes the clutter follows a Gaussian distribution and for each pixel in the image, decides whether an object exists at this particular location or not as follows:

$$(x, y): \begin{cases} \text{target}, & \dfrac{(I_{x,y} - \mu_C)}{\sigma_C} > K_{CFAR} \\ \text{not target}, & \text{otherwise}, \end{cases} \tag{1}$$

where $I_{x,y}$ is the reflectivity at (x,y), μ_C and σ_C are the mean and standard deviation of the clutter reflectivity. As seen from this expression, the ratio on the left-hand side of the inequality is low when there is no target in that pixel and high when there is a target. Since the aim is to stabilize the false alarm rate, the threshold in Equation (1) can be set using the equation below:

$$P_{fa} = \int_{K_{CFAR}}^{\infty} p(r)dr \tag{2}$$

where $p(r)$ is the standard normal probability density function.

In the CA-CFAR approach, the background region, from which the clutter characteristics are learned, is defined as a rectangular region, and a guard region is defined for possible existence of a part of a potential target as seen in Figure 1.
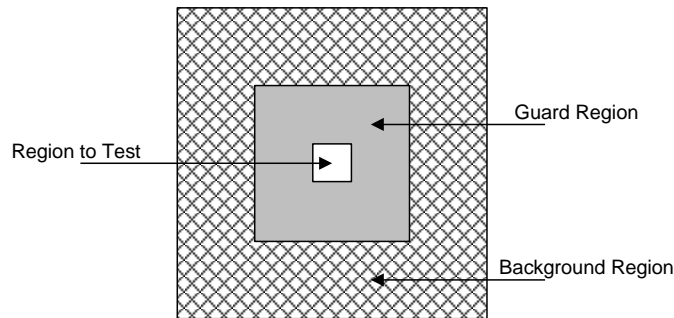

Figure 1 Regions used for learning the clutter statistics in CA-CFAR.

In the CA-CFAR approach, the size of the guard and background regions directly affect the estimated clutter statistics, hence the selection of these regions is critical for the success of the method [5]. In this step, the resolution of the image and the size of the target objects should be taken into account. Hence as the size of the background region increases, the algorithm could be expected to give better detection performance since the clutter characteristics are estimated better. However, the performance of this approach can degrade significantly in the case of nonhomogeneities in the background region or existence of other objects in this region (see Figure 2 for some examples).

In the literature a number of modifications to CA-CFAR have been proposed in order to improve its performance in various scenarios. Ordered statistics CFAR (OS-CFAR) has been proposed to enable detection of closely located objects that cause nonhomogeneities in the background region [3]. For the clutter edge regions, Greatest of CFAR (GO-CFAR) and for multi-target case Smallest of CFAR (SO-CFAR) have been proposed for the clutter edge regions and multi-target case respectively. While all of these techniques produce good results in specific scenarios, they perform worse than CA-CFAR in other cases. This has motivated researchers to develop more flexible and generic, so called adaptive, CFAR algorithms [2], that could offer satisfactory results over a variety of conditions.

| (a) | (b) | (c) | (d) |

| (e) | (f) | (g) | (h) |
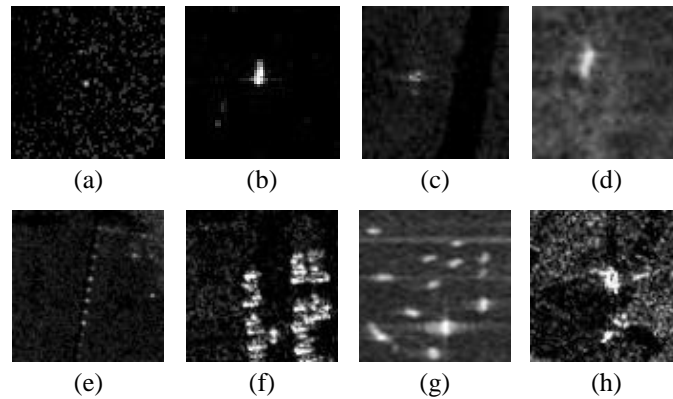
Figure 2 Examples for targets in (a)-(d) homogeneous backgrounds, (e)-(h) nonhomogeneous backgrounds.

With this perspective, Smith and Varshney have proposed Variability Index CFAR (VI-CFAR) [5], which estimates the statistics of the clutter by evaluating a weighted average of the pixels in the background region. It is reported to be successful in both homogeneous and nonhomogeneous regions. Farrouki and Barkat have modified this approach by discarding the pixels of other possible targets in the background regions during the calculation of the clutter statistics and proposed the Automatic Censored CFAR (AC-CFAR) [9].

Although these methods have initially been considered for Gaussian distributed clutter, it is possible to extend them to other types of clutter distributions such as Rayleigh, Weibull, Log-Normal, K. There also exists some body of work focused particularly on one of these clutter distributions [10, 11]. Assuming Weibull clutter distribution, Bisceglie has proposed the solid stencil CFAR algorithm [6] which also involves a number of operations including sorting and censoring, to adapt the background for both homogeneous and nonhomogeneous regions. It has also been proposed to use the beta-prime distribution to handle the nonhomogeneities of the background region and use classical CFAR approach [12] for target detection. However, it is reported that this approach fails for the multi target case since the threshold grows significantly because of the target pixels in the background region.

Ai et al. have proposed an algorithm to detect ship targets using the spatial gray level intensity correlation coefficient, where the clutter is assumed to have a log normal distribution. This method is reported to be unsuitable for point targets by the authors due to the use of strong correlation between neighboring pixels inside the ship target [13]. Gao et al. have proposed an algorithm based on automatic censoring that initially thresholds the image globally to obtain target candidates then scans the image with a sliding window processing only these candidates. This approach decreases the computational cost for parameter estimation of G^0 distribution which is used to model the clutter. The authors provide a simple but effective solution for the computational cost problem of parameter estimation which is a common issue for sliding window techniques. The issue of fixed window size which limits the adaptivity of the approach still remains. Hence targets of different sizes, naturally encountered in SAR images, are still difficult to detect [2]. Zhang et al. have proposed a measure called the polarimetric interferometric eigenvalue similarity parameter (PIESP) which is based on the similarity between two polarimetric SAR images obtained by two interferometric antennas. Polarimetric interferometric systems use two antennas to measure the same ground area with slightly different image geometry. Thus, PIESP can be used to detect the target based on coherence and similarity [14]. Marques et al. focus on the detection of reflective small regions, i.e., point targets, using a level-set based algorithm. Their method incorporates speckle statistics which avoids the need for a despeckling step. The evolving curve in this level-set approach moves outward faster in homogeneous regions following local statistics and differentiating intensity variations [15]. Nar et al. proposed a region based target detection approach which adaptively determines the target shape and clutter regions by utilizing a region growing method [16].

3. PROPOSED METHOD

As mentioned in the previous sections, the aim of this study is to develop a target size and shape independent CFAR approach in order to form a background region that contains sufficient number of clutter pixels for estimation of its statistics. Besides, it is desired to reduce the computational load by reducing the number of candidate target regions, hence the time spent on calculation of the clutter statistics.

Our method consists of a number of algorithmic steps (see Figure 3) starting with despeckling the image so that homogeneous regions are smoothed. The despeckling algorithm can be arbitrary as long as it preserves edges and bright point reflectors while smoothing the homogeneous regions. In the second step, regions which are brighter as compared to their neighbors (regional maxima) in the despeckled image are found and declared as seed regions to initiate the search potential targets . Target region candidates are obtained by growing these seed regions using a region growing algorithm. A candidate target region may have an arbitrary, irregular shape hence the guard and clutter regions enveloping this candidate target region will have similar arbitrary shapes as well since they are constructed by dilating the candidate target region. Possible non-clutter pixels in the clutter regions are censored so that clutter statistics can be obtained in a more robust manner. Clutter statistics are calculated using the original image within the clutter region where Rayleigh, Gamma, Weibull, Log-Normal, K or any other clutter distribution can be used. Decision of possible target regions, either target or non-target, is made using the maximum intensity of that candidate target region using an adaptive threshold value which satisfies a CFAR constraint. We call this approach region based CFAR (RB-CFAR).

Computational requirements of the proposed method are low due to three reasons: a) possible candidate regions constitute a small percentage of the overall scene; b) a single hypothesis test is performed for all the pixels in each region therefore their clutter statistics are calculated only once; and c) efficient and parallelizable algorithms are used for each step of the proposed method. Computation time also depends on the choice of despeckling method, clutter size and clutter distribution. For example, clutter distributions such as Gamma require heavy computations for adaptive threshold selection. In the following subsections, we describe each step of our approach in more detail.
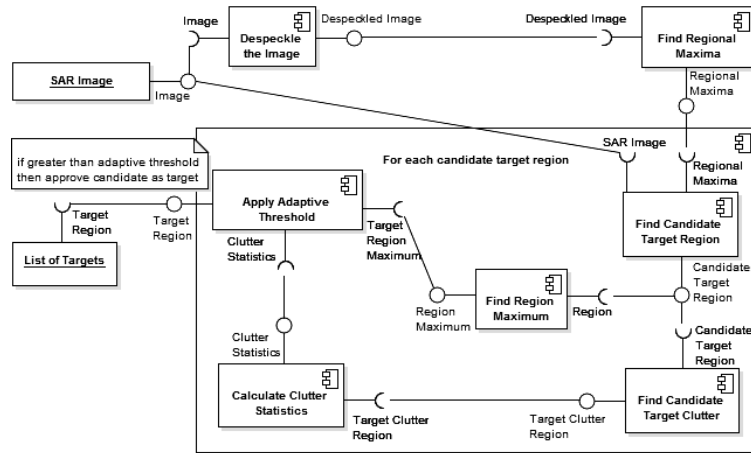

Figure 3 Block diagram of the proposed RB-CFAR method.

3.1 Despeckling of SAR Images

First a filtered image is obtained using a despeckling method which preserves edges and bright point reflectors while smoothing the homogeneous regions. Despeckling is very critical since there may be huge number of regional maxima and candidate target regions if homogeneous regions are not sufficiently smoothed. We suggest the following guidelines for choosing a despeckling method:

- Despeckling performance

    A despeckling method performs well for our needs if it smoothes homogenous regions while preserving edges and bright point reflectors. If the despeckling method over-smoothes edges or bright point reflectors, such targets may be missed in the target detection step.

- Availability of an already despeckled image

  Despeckling is generally a common first step in various SAR image processing algorithms or tasks in a SAR image exploitation system. Hence a despeckled image may have already been prepared for other tasks such as image segmentation, classification, or target recognition. Therefore, one may prefer to use this pre-computed result if it fits the requirements of the proposed method.

- Computational requirements

  Despeckling methods have different computational loads and execution durations. Their computation time can be fixed if a convolution kernel is used or indefinite if an iterative approach with a convergence criterion is used. Long or indefinite running times may not be suitable for time-critical systems.

- Impact on computational load for further steps

  The despeckled image is used in the process of finding regional maxima and target candidates (See Sections 3.2 and 3.3). If the despeckling method smoothes homogenous regions successfully then the number of false target candidate regions will be reduced and this will decrease the computation time of further steps. Generally speaking, we may prefer a despeckling method that is somewhat computationally demanding, for the sake of obtaining better despeckling performance. While this could increase the execution time for despeckling itself, it might decrease the overall computational load of the ATD system as it has the potential to decrease the required duration for further steps thanks to effectively smoothed homogonous regions and reduced number of false target candidate regions .

In this study, feature preserving despeckling (FPD), [17][18], and enhanced Frost [19] methods are used for SAR image despeckling to show the impact of despeckling method on further algorithmic steps in terms of speed and accuracy. As seen in Figure 4, FPD performs better as compared to enhanced Frost filter, while computation is slower in the two orders of magnitude. To alleviate the computational burden of FPD, we have developed a parallel GPU implementation in which the computation time is reasonable, but is still one order of magnitude larger as compared to parallel CPU implementation of enhanced Frost. Details of GPU and CPU parallelizations of FPD and enhanced Frost are provided in Section 3.7.

In FPD the SAR image denoising problem is posed as an optimization problem:

$$\hat{f} = \arg \min_{f} J(f) \tag{3}$$

where the cost function $J(f)$ is defined as:

$$J(f) = \left\| g - f \right\|_2^2 + \lambda_1^2 \left\| f \right\|_k^k + \lambda_2^2 \left\| Df \right\|_k^k \tag{4}$$

where g is the observed, speckled SAR image, $\|.\|_k$ denotes the l_k norm, D is the 2-D derivative operator, f is the noise-free reflectivity image of the scene, and λ_1 and λ_2 are scalar parameters. The first term of the objective function is the data fidelity term; the second and third terms are for enhancing point based and region based features, respectively. This cost function has been obtained as a simplified version of the cost function used in the feature-enhanced SAR imaging approach of [17]. FPD parameter k is set to 1 due to its good edge preserving characteristics, λ_1 is set to zero since there is no need to enhance the point based features for our despeckling objectives, and λ_2 is set to 12 which is tuned for 16 bit TerraSAR-X strip mode and TerraSAR-X high resolution spotlight mode sample SAR images (downloadable from TerraSAR-X web site free of charge) [21]. Speckle noise in Figure 4(a) is successfully removed using FPD as seen in Figure 4(b).

The Frost filter is based on an exponential kernel whose parameters include the local coefficient of variation [20]. Hence, the filter is in between an all pass filter and an averaging filter depending on the coefficient of variation in the kernel window. Lopes et al. have introduced some modifications to Lee and Frost filters by use of two thresholds on the coefficient of variation [19] which is called enhanced Lee and enhanced Frost. Enhanced Frost filter parameter K is set to 0.5 and kernel size is chosen as 5x5 so that homogenous regions are smoothed. In Figure 4(c) the enhanced Frost despeckling result is shown. As seen in Figure 4, FPD exhibits better preservation of regions and point targets while smoothing homogenous regions more effectively compared to enhanced Frost.

| a) Original SAR image | b) FPD despeckled | c) Enhanced Frost despeckled |
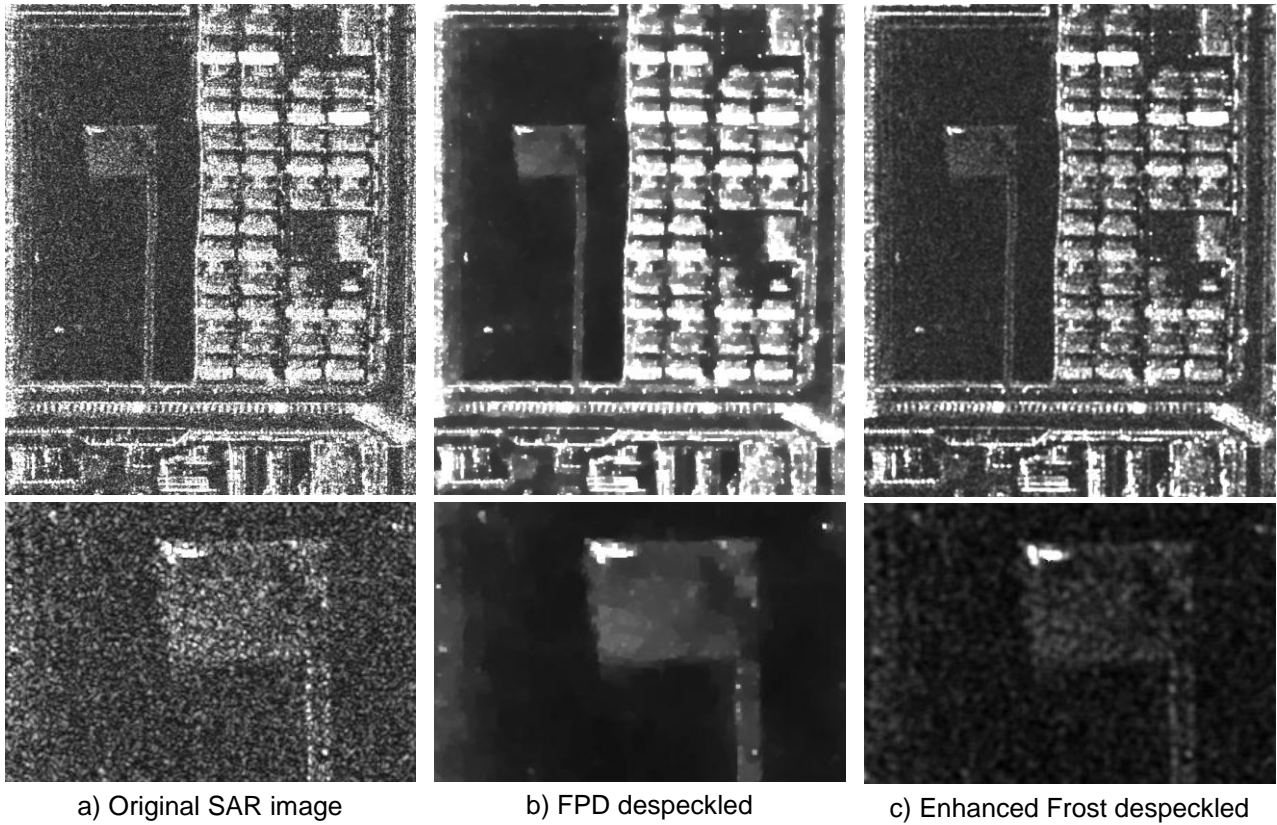
Figure 4 SAR image despeckling results.

3.2 Determination of Regional Maxima

Potential target candidates have greater intensity values compared to their neighbors in a despeckled image (see Figure 4). Based on that observation, regional maxima within the despeckled image are found. A regional maximum is defined as a group of connected pixels with the same intensity value that is greater than the intensities of pixels in the neighboring regions [22]. For defining regions and region boundaries either 4 or 8 connectedness can be used. In this study 8-connectedness is used since there may be diagonally connected sub regions within a region. In Figure 5, regional maxima are illustrated with bold numbers where numbers corresponds to intensity values in an image.

Figure 5 Illustration of regional maxima.

Regional maxima cover only a small percentage of SAR images as seen in Figure 6(c) and Figure 6(e). The percentage of regional maxima is roughly 2.8% for our test dataset composed of 65 TerraSAR-X images. Despeckling of the image is important since speckle noise causes additional regional maxima which will in turn result in a large number of false candidate target region seeds. FPD leads to formation of better regional maxima, therefore it also leads to formation of better candidate target regions compared to enhanced Frost (see Figure 6).
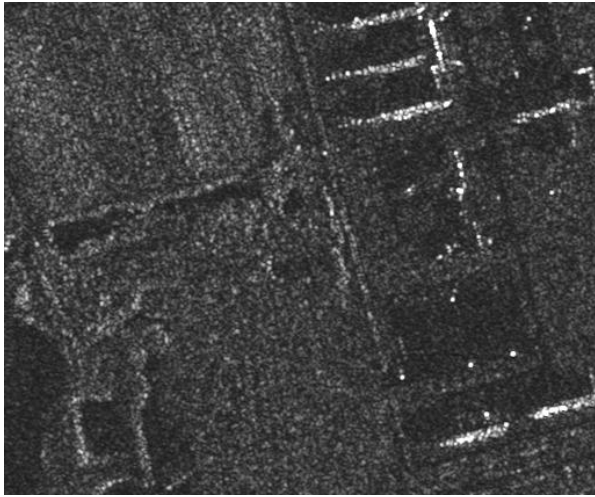
a) SAR image
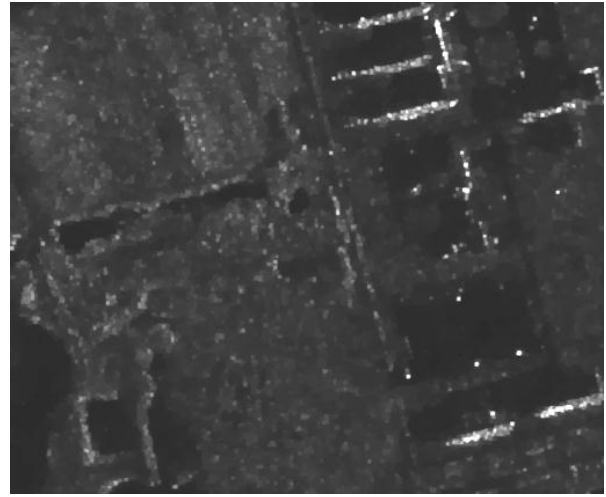
b) FPD filtered SAR image
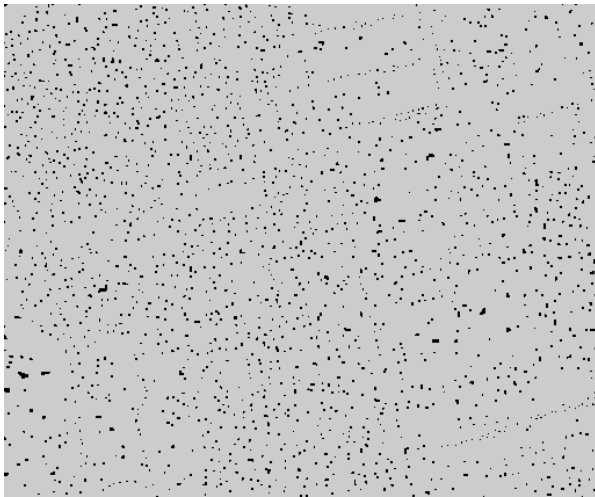
c) Regional maxima on FPD result
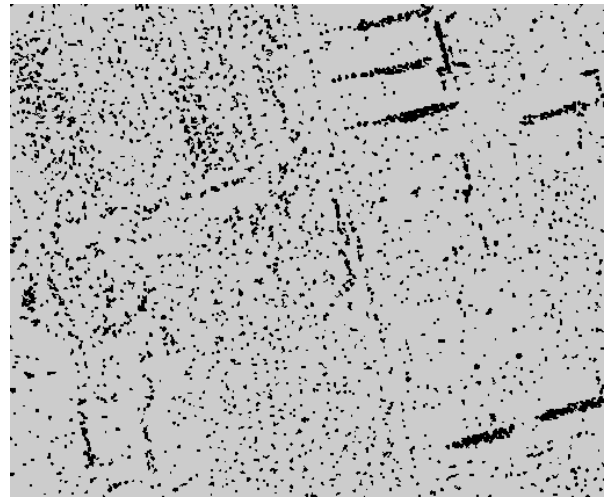
d) Candidate target regions for (c)
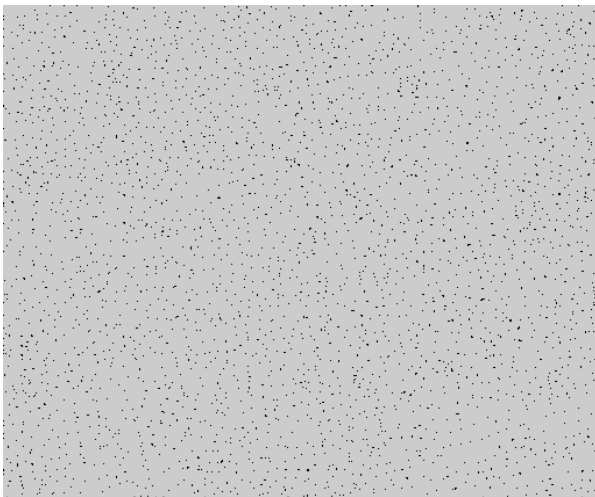
e) Regional maxima on enhanced Frost result
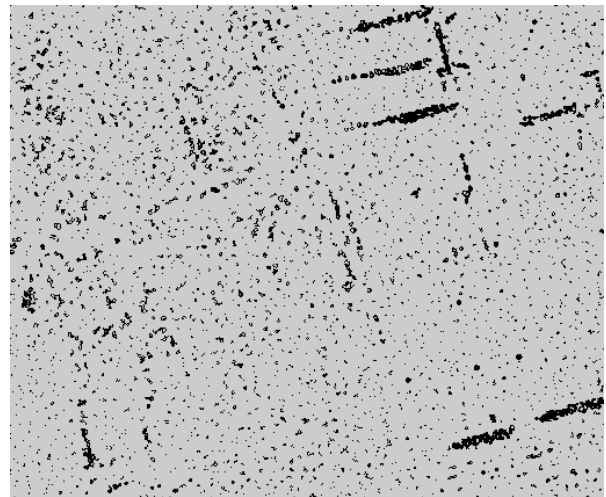
f) Candidate target regions for (e)

Figure 6 Candidate target region determination steps.

3.3 Growing Regional Maxima as Candidate Targets

Regional maxima are expanded using a region growing algorithm and turn into target candidate regions where multiple regional maxima can merge and become a single region. Each region is expanded by adding pixels connected to the region boundary having sufficient similarity with the region center mean until no similar pixels are found (Figure 7). Region center mean C_μ is recalculated whenever a pixel is added to the region until region becomes large enough (16 pixels in our experiments).
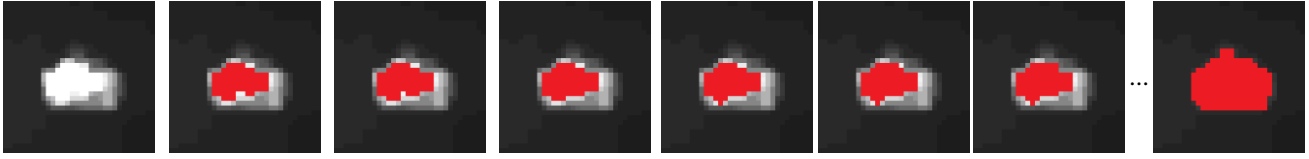
Figure 7 Sample region growing iterations.

In Figure 8, the histogram of a 12-bit SAR image histogram is shown as a probability density function (PDF) estimate. As seen in this histogram SAR images have high dynamic range, and for 16-bit SAR images the dynamic range is even higher. Due to this high dynamic range, use of linear pixel similarity measures within region growing will cause region growing to fail since the similarity measure used for higher intensity values will cause rapid expansion of the region for lower intensity values. To alleviate this problem, the cumulative distribution function (CDF) is estimated based on the histogram, and a pixel similarity metric is defined using CDF values of two intensities as given in Equation (5).

(a) Histogram-based PDF estimate. (b) Histogram-based CDF estimate.
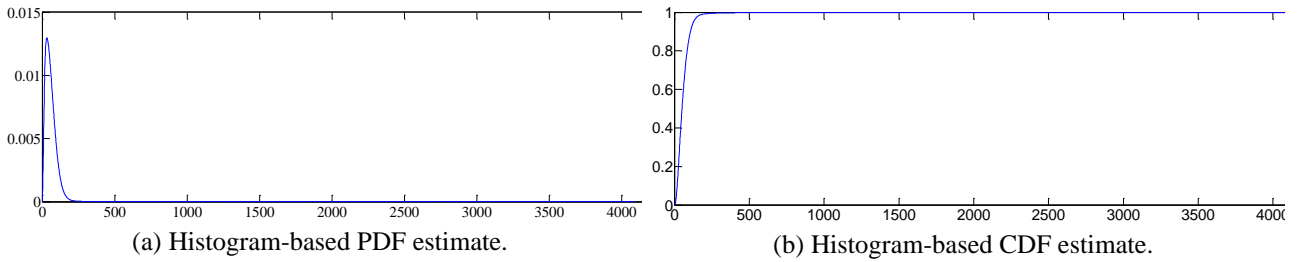
Figure 8 SAR image histogram-based PDF and CDF estimates.

Pixel similarity measure ($S_{C_\mu, I_{x,y}}$) and pixel distance measure ($D_{C_\mu, I_{x,y}}$) within our region growing are defined as:

$$S_{C_\mu, I_{x,y}} = -D_{C_\mu, I_{x,y}} \tag{5}$$

and

$$D_{C_\mu, I_{x,y}} = \left| CDF_{C_\mu} - CDF_{I_{x,y}} \right| \tag{6}$$

where $I_{x,y}$ is the intensity value of a pixel connected to region boundary, C_μ is region center mean, $CDF_{I_{x,y}}$ is the CDF of the intensity value $I_{x,y}$, and CDF_{C_μ} is CDF of the intensity value C_μ. Pixels connected to the region boundary having $D_{C_\mu, I_{x,y}}$ values less than a distance threshold are added to a priority queue with their similarity value as their priority. In this study, the distance threshold is set to 0.025 which is experimentally determined. The region is expanded using the pixels in the priority queue which leads to more natural expansion of regions where pixels with higher priority values are retrieved first.

Region growing is also limited to pixels having intensity values between the lower and upper intensity limits to prevent uncontrollable expansion of regions. Lower intensity limit is the first intensity value where CDF becomes equal to or larger than 0.05, which means pixels with lowest 5% intensities of the image are excluded from region growing. Intensity value of the regional maxima is used as the upper intensity limit. Target candidate regions found by region growing are still a small percentage (6.9%) of the image which leads to computational efficiency for further steps.

3.4 Finding Guard and Clutter Regions

Candidate target regions are expanded by a guard radius; with a default value of 2 this expanded region is called the guard region. Similar to existing CFAR methods, the guard region is used for preventing target pixels to be mixed in the clutter region. The guard region area depends on the candidate target size and shape since the guard region is obtained by dilating the candidate target region. The RB-CFAR method requires smaller guard area as compared to traditional CFAR methods since the target region shape and the guard shape are adaptively found. This approach helps the RB-CFAR method to collect more clutter data especially for the targets having other targets in their close neighborhood since such targets will be censored from clutter region. The guard region is further expanded by clutter radius, with a default value of 5 This further expanded region is called the clutter region. In Figure 9 black pixels in inner regions correspond to candidate target regions, outer regions correspond to clutter regions and middle regions corresponds to guard regions. As seen in Figure 9(a) the target candidate region may have a very simple shape or as seen in Figure 9(d) and Figure 9(e) it may also have a very complex shape. As seen in Figure 9(c), during dilation operation other candidate target regions are censored so that the possibility of the clutter region containing non-clutter pixels is reduced.

a) Single pixel target   b)   c)   d)   e)

Figure 9 Candidate target region, guard region, and clutter region examples.

3.5 Calculating Clutter Statistics

In SAR images, the statistics of the cutter vary excessively depending on the nature of the background region and there exists extensive research on statistical modeling of clutter in SAR images [14]. These studies show that the characteristics of the speckle noise in the image depend on the land cover: in general the clutter fits Rayleigh distribution on sea surface, Gamma distribution on empty land or farmland and Weibull distribution on urban areas. There are also some generalized distributions like K or G_0 distributions that have found use in the literature. In this study only the Rayleigh and Gamma distributions are utilized to demonstrate the performance of the method.

The PDF of the Rayleigh distribution is given by:

$$p(x) = \frac{x}{b^2} e^{-\frac{(x)^2}{2b^2}} \tag{7}$$

This distribution is parameterized by only one parameter and this parameter can be estimated as shown in Equation (8), where x_i's are the reflectivities of the clutter pixels and the CFAR threshold is evaluated by Equation (9) which can be derived using Equation (2).

$$\hat{b} = \sqrt{\frac{1}{2N} \sum_{i=1}^{N} (x_i)^2} \tag{8}$$

$$\tau = \sqrt{-2\hat{b}^2 \ln(P_{FA})} \tag{9}$$

The PDF of the Gamma distribution is given by:

$$p(x) = \frac{1}{\beta^\gamma \Gamma(\gamma)} x^{\gamma-1} e^{-\frac{x}{\beta}} \tag{10}$$

The parameters of this distribution are also estimated using the pixels in the clutter region as shown in Equation (11) and the CFAR threshold is found using Equation (12).

$$\hat{\beta} = \frac{\hat{\sigma}^2}{\mu}, \quad \hat{\gamma} = \frac{\hat{\mu}}{\hat{\beta}}$$

$$\hat{\mu} = \frac{1}{N} \sum_{i=1}^{N} \ln(x_i) \tag{11}$$

$$\hat{\sigma}^2 = \frac{1}{N-1} \sum_{i=1}^{N} (\ln(x_i) - \mu)^2$$

$$\tau = \hat{\beta} \cdot \Gamma^{-1}(\hat{\gamma}, P_{FA}) \tag{12}$$

where $\Gamma(\gamma, x)$ is the Incomplete Gamma function.

3.6 Applying an Adaptive Threshold

If the clutter region does not contain enough samples (less than 64 pixels in our experiments) then this candidate target region is assumed to be a clutter region. Otherwise, as the final step, calculated CFAR threshold is applied to the candidate targets. Since the candidate targets are formed using region growing and involve both large and small scatterers, comparing the mean reflectance of the candidate targets with the threshold could lead to loss of the target. Hence, in this study we propose to use the maximum reflectance value in each candidate target region to compare with the CFAR threshold and declare that region as target if its maximum reflectance is greater than the threshold, and as clutter otherwise.

3.7 Parallel Implementations

Parallel processing has become a key element to speed up scientific computations. Accordingly, parallelizable algorithms are used for each step of the proposed method and OpenMP for CPU and NVidia CUDA for GPU are used for actual implementations. Finding regional maxima, region growing for finding candidate target regions, and finding clutter regions steps require efficient implementation of bit-plane pixel state representation. If 8-bits pixel format is used then threads need to be divided into four groups such that the 0th thread uses the first 2-bits; the 1st thread uses the second 2-bits; the 2nd thread uses the third 2-bits;the 3rd thread uses the last 2-bits; the 5th thread uses the first 2-bits again, and it goes on like that. Especially in regional maximum step, the non-maxima regions are dynamically divided into smaller regions so that the 1st thread and the 5th thread do not access the same image regions which would potentially result in memory read and write hazards.

In Table 1, the computation times of the algorithmic steps of our approach are given for 3.07 GHz 4-cores i7 CPU and Nvidia GTX 460 1.55 GHz 336-cores GPU implementations. Despeckling is the most time consuming part of the proposed method where GPU based FPD took 63 seconds and 8-threads CPU based enhanced Frost took 6.4 seconds. We speculate that , with the recently introduced Nvidia Keppler series, the current 63 seconds computation time of FPD will decrease to around 15 seconds. As seen in Table 1, the fastest execution mode of RB-CFAR would use GPU based FPD for despeckling (63 seconds) and 8-threads CPU implementations for the others steps (6.5 seconds).

Table 1 Computation time of algorithmic steps for 10 images with the approximate size of 16000x16000

Algorithm Step (in seconds)	1-thread	2-threads	4-threads	8-threads	GPU
(Section 3.1) Despeckling (using FPD)	2136.0 sec	1134.0 sec	964.0 sec	743.0 sec	63 sec
(Section 3.2) Regional Maxima	7.7 sec	5.6 sec	3.1 sec	2.4 sec	-
(Section 3.3) Finding Candidate Target Regions	3.4 sec	2.2 sec	1.2 sec	1.0 sec	-
(Section 3.4) Finding Clutter Regions	12.3 sec	5.7 sec	4.6 sec	2.8 sec	-
(Section 3.5) Calculating Clutter Statistics (for Rayleigh)	0.6 sec	0.4 sec	0.3 sec	0.3 sec	-
(Section 3.5) Applying an adaptive threshold	negligible	Negligible	negligible	negligible	-

4. EXPERIMENTAL RESULTS

In Figure 10 and Figure 11 target detection results for the proposed method (RB-CFAR), CA-CFAR, and AC-CFAR are shown for various targets including an isolated ship on sea, multiple ships alongside the quay, a bridge, POLs, tall buildings, a short building surrounded by farmland, lifting cranes, a power pole, and a railroad. Identical region growing parameters, guard radius, and clutter radius are used for all the RB-CFAR results where for the other methods all the parameters are fine-tuned in each case. These results show that RB-CFAR provides computational efficiency for detecting targets in different size and shape in a single execution with good detection accuracy and low false alarm rates.

700x700, 1m, Rayleigh, $p_{fa}=10^{-6}$	RB-CFAR	CA-CFAR	AC-CFAR
1350x1350, 1m, Rayleigh, $p_{fa}=10^{-6}$	RB-CFAR	CA-CFAR	AC-CFAR
400x400, 1m, Rayleigh, $p_{fa}=10^{-6}$	RB-CFAR	CA-CFAR	AC-CFAR
350x350, 1m, Rayleigh, $p_{fa}=10^{-6}$	RB-CFAR	CA-CFAR	AC-CFAR
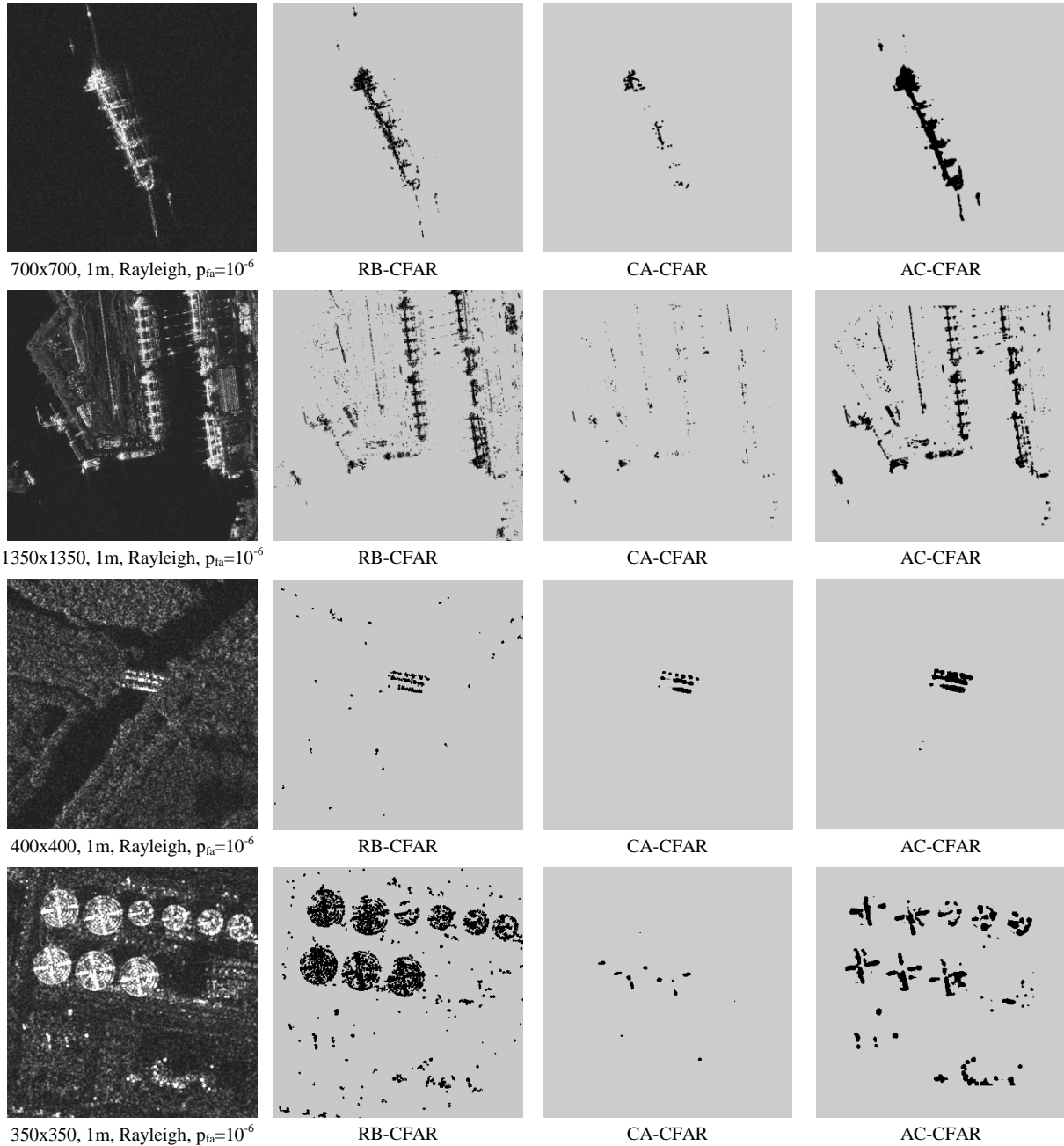
Figure 10 Results of the RB-CFAR, as well as CA-CFAR and AC-CFAR methods.

450x450, 1m, Rayleigh, $p_{fa}=10^{-6}$ RB-CFAR   CA-CFAR   AC-CFAR
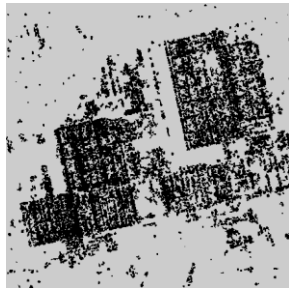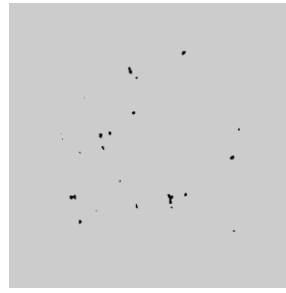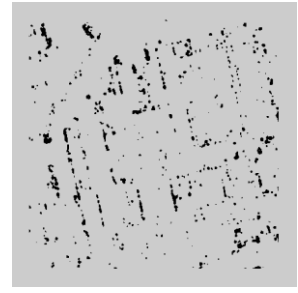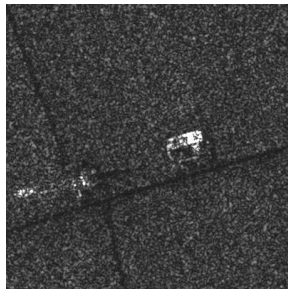
400x400, 1m, Gamma, $p_{fa}=10^{-4}$ RB-CFAR   CA-CFAR   AC-CFAR
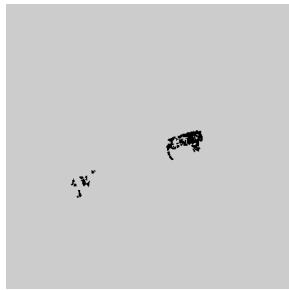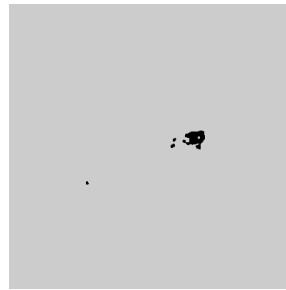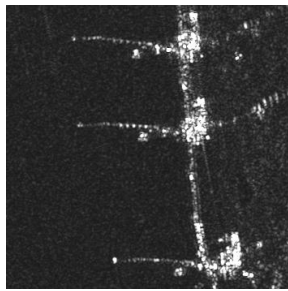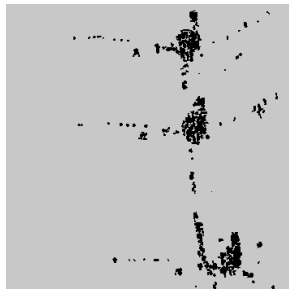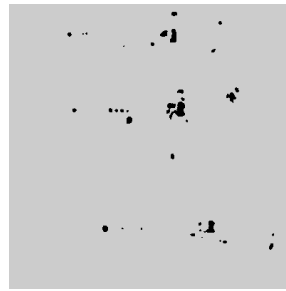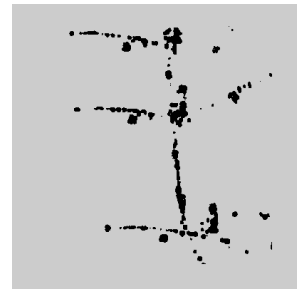
400x400, 1m, Rayleigh, $p_{fa}=10^{-6}$ RB-CFAR   CA-CFAR   AC-CFAR
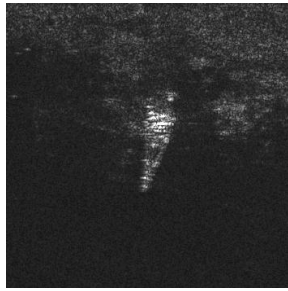
350x350, 0.33m, Rayleigh, $p_{fa}=10^{-6}$ RB-CFAR   CA-CFAR   AC-CFAR
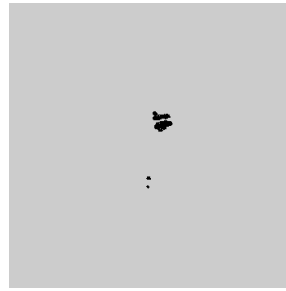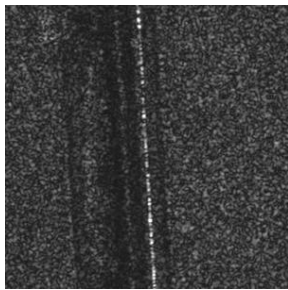
300x300, 1m, Rayleigh, $p_{fa}=10^{-6}$ RB-CFAR   CA-CFAR   AC-CFAR
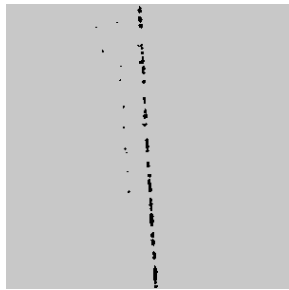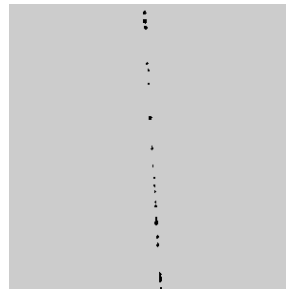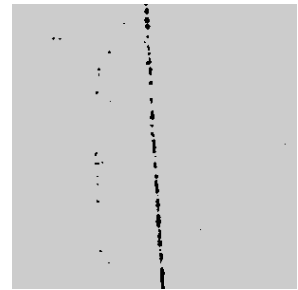
Figure 11 Results of the RB-CFAR, as well as CA-CFAR and AC-CFAR methods.

As seen in the Figure 12, man-made structures having high variety in size, shape, reflectivity, background homogeneity, clutter type, proximity to other man-made structures are successfully detected.
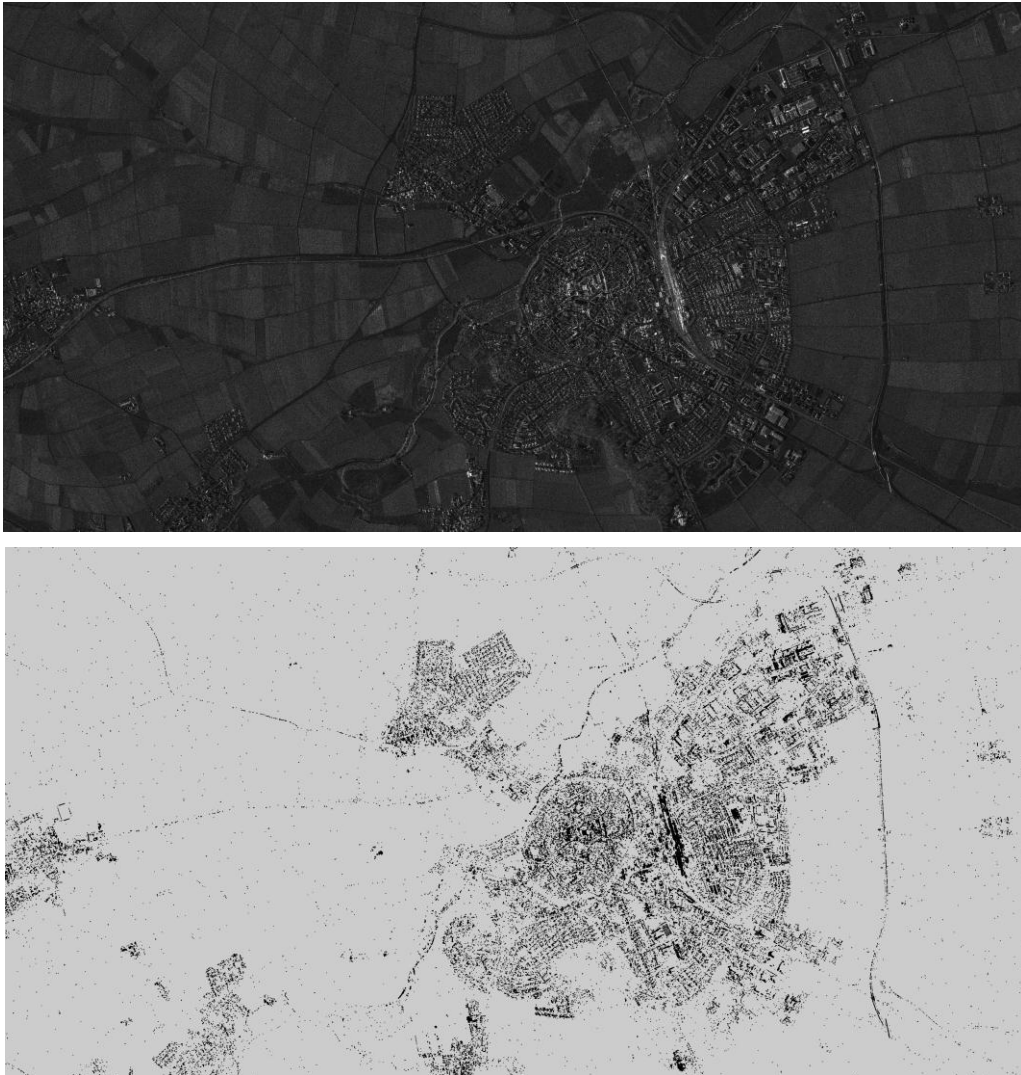

Figure 12 Man-made detection result of the RB-CFAR for Nördlingen town in Holland.

5. CONCLUSION

In this study, a novel CFAR method is proposed which can perform target detection independent of image resolution and target shape and size even in heterogeneous background clutter. As the first merit, the proposed method adaptively determines the target shape and the surrounding clutter regions by utilizing a region growing method and performing hypothesis testing based on the background model. Through this procedure, it is possible to detect various types of targets having different shapes and sizes. As a second merit, the proposed method allows fast target detection since a) clutter statistics are calculated only for candidate target regions which cover a small percentage of the image, b) only a single execution of the method is sufficient for detecting different type of targets having different shapes and sizes, and c) each step of the proposed method is parallelized using OpenMP for CPU and NVidia CUDA for GPU implementations. Our experimental results on a diverse set of images demonstrate the effectiveness of the proposed approach.

REFERENCES

[1]   Ross, T. D. "SAR ATR - So what's the problem? - An MSTAR perspective," Algorithms for Synthetic Aperture Radar Imagery Vi, vol. 3721, pp. 662-672, (1999).

[2]   Gao, G., Liu, L., Zhao, L., Shi, G., Kuang, G., "An Adaptive and Fast CFAR Algorithm Based on Automatic Censoring for Target Detection in High-Resolution SAR Images," IEEE Trans. on Geoscience and Remote Sensing, vol. 47, pp. 1685-1697, (2009).

[3]   Novak, L.M., Hesse, S. R., "On the Performance of Order-Statistics Cfar Detectors," Conference Record of the Twenty-Fifth Asilomar Conference on Signals, Systems & Computers, vols 1 and 2, pp. 835-840, (1991).

[4]   R. Chellappa, "Understanding Synthetic Aperture Radar Images," Proceedings of Image Understanding Workshop, pp. 229-247, (1992).

[5]   Smith M. E., Varshney, P. K. "VI-CFAR: A novel CFAR algorithm based on data variability," Proceedings of the 1997 IEEE National Radar Conference, pp. 263-268, (1997).

[6]   Bisceglie M., Galdi, C., "CFAR Detection of Extended Objects in high-resolution SAR images," IEEE Transactions on Geoscience and Remote Sensing, vol. 43, pp. 833-843, (2005).

[7]   Siddiq, K., "Performance of the VI-CFAR in homogeneous Weibull background," 10th IEEE International Multitopic Conference 2006, Proceedings, pp. 309-313, (2006).

[8]   Novak, L.M., "The automatic target-recognition system in SAIP," Lincoln Laboratory Journal, vol. 10, 1997.

[9]   Farrouki A., Barkat, M., "Automatic censoring CFAR detector based on ordered data variability for nonhomogeneous environments," IEE Proceedings-Radar Sonar and Navigation, vol. 152, pp. 43-51, Feb 2005.

[10]   Wang, C., Liao, M., Li, X., "Ship detection in SAR Image Based on the Alpha-stable Distribution," Sensors, vol. 8, pp. 4948-4960, (2008).

[11]   Erfanian S., Vakili, V.T., "Introducing Excision Switching-CFAR in K distributed Sea Clutter" Signal Processing, Vol. 89, pp. 1023-1031, (2009).

[12]   Frery, A. C., "A model for Extremely Heterogeneous Clutter," IEEE Transactions on Geoscience and Remote Sensing, vol. 35, pp. 648-659, (1997).

[13]   Ai, J., Qi, X., Yu, W., Deng, Y., Liu, F., Shi, L., "A New CFAR Ship Detection Algorithm Based on 2-D Joint Log-Normal Distribution in SAR Images", IEEE Geoscience and Remote Sensing Letters, Vol. 7, No. 4, (2010).

[14]   Zhang, L., Zou, B., Wenyan, T., "Polarimetric Interferometric Eigenvalue Similarity Parameter and Its Application in Target Detection", ", IEEE Geoscience and Remote Sensing Letters, Vol. 8, No. 4, (2011).

[15]   Marques, R.C.P., Sombra de Medeiros, F.N., Ushizima, D.M., "Target Detection in SAR Images Based on a Level Set Approach", IEEE Transaction on Systems, Man, and Cybernetics – Part C: Apllications and Reviews, Vol. 39, No. 2, (2009).

[16]   Nar, F., Demirkesen, C., Okman, O.E., Cetin, M., "A Region Based Target Detection Method for SAR Images", in IEEE 19th Conference on Signal Processing and Communications Applications (SIU), pp. 809-812, 20-22 (2011).

[17]   Çetin, M., Karl, W., C., "Feature Enhanced Synthetic Aperture Radar Image Formation Based on Nonquadratic Regularization", IEEE Transactions on Image Proccess, Vol. 10, No. 4, pp. 623-631, (2001).

[18]   Okman, O.E., Demirkesen, C., Nar, F., Cetin, M., "Feature Preserving Despecklind and Its Parallel Implementation with Application to Railway Detection", to be appear in IEEE 9th European Conference on Synthetic Aperture Radar (EUSAR), (2012).

[19]   A. Lopes, R. Touiz and E. Nezry, "Adaptive speckle filters and scene heterogeneity", IEEE Transaction on Geoscience and Remote Sensing, vol. 28(6), pp. 992-1000, Nov (1990).

[20]   Frost, V.S., Stiles, J.A., Shanmugan, K.S., Holtzman, J.C., "A Model for Radar Images and Its Application to Adaptive Digital Filtering of Multiplicative Noise", IEEE Transactions of Pattern Analysis and Machine Intelligence, Vol 4(2), pp 157-166, (1982).

[21]   TerraSAR-X Archive, 2011, terrasar-x-archive.infoterra.de

[22]   Dougherty, E.R., Lotufo, R.A., "Hands-on Morphological Image Processing", SPIE Tutorial Texts in Optical Engineering, (2003).